The electron transfer kinetics of adsorbed species derived by sampled current voltammetry

Oliver Rodríguez, Guy Denuault*

Chemistry, University of Southampton, Southampton, SO17 1BJ, UK.

Abstract

In sampled current voltammetry, a sampled current voltammogram (SCV) is constructed by performing a number of potential steps and plotting the currents taken at a specific sampling time against the corresponding step potentials. For diffusion-controlled processes, the technique produces sigmoidal current-potential curves that are easily analysed to obtain kinetic information. Here, we extend this approach to study the electron transfer kinetics of adsorbed species ($O_{ads} + ne^- \underset{k_b}{\overset{k_f}{\rightleftharpoons}} R_{ads}$) and show that the SCVs have a characteristic peak whose shape, potential and current depend on the sampling time. We also discuss the results in terms of chronocoulograms and show that the sampled charge voltacoulograms (SQVs) are also affected by kinetics. Analysis of the SCVs and SQVs is particularly useful to unravel the dependence of the electrode response on potential and time. We investigate different data treatments and show that a logarithmic SCV, a plot of $\ln(j)$ against E, is highly sensitive to the electron transfer rate constant and to the sampling time. The time dependence of the current yields Γ_O^0 (initial surface coverage) and E^0, while the potential dependence of the current extrapolated to very short sampling times yields α and k_s. This extrapolation bypasses the double layer charging distortion, provided the sampling times are selected where the current transients are free from capacitive distortion. From the analysis of the SCVs, we propose a simple protocol to derive Γ_O^0, E^0, α and k_s, from only two current transients, the only constraint being that one of the chronoamperograms must be recorded with a large overpotential, circa ± 120 mV. We also propose a simpler alternative involving non-linear regression of the current transients to a single expression. The chronoamperometric approach offers advantages compared to the voltammetric methodology proposed by Laviron. 1) Capacitive distortions only affect the current transients at short times but affect the whole potential window in voltammetry. 2) The current transients can be extrapolated to very short sampling times where the backward reaction has no influence. 3) The extrapolation to very short sampling times bypasses the double layer distortion. 4) Whereas a chronoamperogram holds a wide range of timescales, the voltammetric approach requires a wide range of scan rates to distinguish the kinetic regimes. 5) The voltammetric method only yields the values of k_s and α, while the chronoamperometric method also yields Γ_O^0 and E^0. 6) Since electrochemical workstations allow shorter time scales by chronoamperometry than voltammetry, the method can asses faster electron transfer kinetics than conventional cyclic voltammetry.

Keywords: sampled current voltammetry, SCV, sampled charge voltacoulommetry, SQV, electron transfer kinetics

1. Introduction

The electrochemical kinetics of adsorbed species is usually studied with the methodology proposed by Laviron, where linear sweep voltammograms are recorded over a range of scan rates ν and the peak potential is plotted against $\ln(\nu)$ [1]. This approach assumes that the species are irreversibly adsorbed, that the coverages for O and R follow a first order rate law and that the rate constant depends on potential according to Butler-Volmer kinetics. Other methodologies based on current transient and differential techniques have also been reported but their implementation and the analysis needed to extract kinetic information are unwieldly [2, 3, 4, 5, 6, 7].

Voltammetric techniques are easy to implement and visually descriptive, however, the double layer contribution affects the whole potential window; it is generally subtracted assuming that the charging current is constant over the potential window of interest [8]. It is however often the case that the capacitance of the adsorbed layer varies with the redox state of the adsorbed species [9, 10], the subtraction procedure may thus lead to an erroneous coverage of adspecies. In contrast, potential step techniques are less visually powerful and the extraction of kinetic information (and coverage) is generally cumbersome. Their advantage is that the double layer charging current decays exponentially with time thus leaving the Faradaic current undis-

*Corresponding author
Email address: gd@soton.ac.uk (Guy Denuault)

torted once the double layer charging process is complete. The Faradaic current also decays exponentially with time but with a larger time constant dependent on the electron transfer kinetics, *vide infra*. The timescale of the charging process can even be significantly shortened with the use of microelectrodes and this has been exploited to study very fast processes [9, 11, 12, 13]. In this study, we show that if the current transients are recorded for different target potentials, the corresponding sampled current voltammograms provide a powerful means to visualise kinetic limitations. We then exploit the underpinning theory and develop two simple protocols to derive kinetic information.

In sampled current voltammetry, chronoamperograms are first recorded for a number of target potentials within the potential range of interest. Currents from the resulting (E, t, j) dataset are then sampled at a specific time and plotted against the corresponding target potentials to create one SCV. Sampling the chronoamperograms at other times produces a family of SCVs, and this is the main difference with normal pulse voltammetry: whereas normal pulse voltammetry produces only one SCV by recording the current at a preselected time, sampled current voltammetry acquires whole chronoamperograms and generates a family of SCVs. Sampled current voltammetry has been used sporadically to study diffusion controlled species, mostly by sampling at long times to obtain a quasi-steady state response [14, 15, 16]. However, the ability to extract information at different time scales is an important feature of sampled current voltammetry. Our group demonstrated this by exploiting sampled current voltammetry to extract kinetic information from the different diffusion regimes obtained with microdisc electrodes [16, 17]. Recently, we have used sampled current voltammetry to investigate electrochemical kinetics on surfaces unsuitable for rotating discs or microelectrodes [18]. Here, we extend the work reported in [16] and develop the theory of sampled current voltammograms for adsorbed species, e.g. self-assembled osmium complexes [9, 10], chemisorbed ferrocene [4] or anthraquinone [6, 12].

In Section 2, we develop the theoretical expressions for the SCVs and sampled voltacoulograms (SQVs). In Section 3, we analyse the shape of the SCVs and SQVs. In Section 4, we discuss experimental issues and investigate different procedures to extract the kinetic information and coverage from the datasets.

2. Theory

The following reaction where O and R are both adsorbed on the electrode surface is assumed:

$$\mathrm{O_{ads}} + n\mathrm{e}^- \underset{k_b}{\overset{k_f}{\rightleftharpoons}} \mathrm{R_{ads}} \tag{1}$$

where the equilibrium is controlled by the relative magnitude of the forward and backward rate constants, k_f and k_b respectively. Assuming a first order reaction, the differential equation describing the dependence of the coverage of O on time is:

$$\frac{\mathrm{d}\Gamma_{\mathrm{O}}^t}{\mathrm{d}t} = -k_f\Gamma_{\mathrm{O}}^t + k_b\Gamma_{\mathrm{R}}^t \tag{2}$$

It is also assumed that at $t = 0$ the coverage of O in mol cm^{-2} is given by Γ_{O}^0 and that $\Gamma_{\mathrm{R}}^0 = 0$, so that at any given time:

$$\Gamma_{\mathrm{O}}^t + \Gamma_{\mathrm{R}}^t = \Gamma_{\mathrm{O}}^0 \tag{3}$$

With these definitions, the differential equation becomes:

$$\frac{\mathrm{d}\Gamma_{\mathrm{O}}^t}{\mathrm{d}t} = -k_f\Gamma_{\mathrm{O}}^t + k_b(\Gamma_{\mathrm{O}}^0 - \Gamma_{\mathrm{O}}^t) \tag{4}$$

Rearranging and defining $K_\Sigma = k_f + k_b$ yields:

$$\frac{\mathrm{d}\Gamma_{\mathrm{O}}^t}{\mathrm{d}t} = -K_\Sigma\Gamma_{\mathrm{O}}^t + k_b\Gamma_{\mathrm{O}}^0 \tag{5}$$

After solving, see Section 1 of the supporting information for the full derivation:

$$\Gamma_{\mathrm{O}}^t = \frac{k_b\Gamma_{\mathrm{O}}^0 + k_f\Gamma_{\mathrm{O}}^0\exp(-K_\Sigma t)}{K_\Sigma} \tag{6}$$

Equation 6 describes the coverage of O as a function of time. Since the charge passed reflects the coverage of R:

$$Q = nF\Gamma_{\mathrm{R}}^t = nF(\Gamma_{\mathrm{O}}^0 - \Gamma_{\mathrm{O}}^t) \tag{7}$$

Introducing Equation 6 and defining $Q^0 = nF\Gamma_{\mathrm{O}}^0$, the charge passed is now:

$$Q = Q^0\Big[1 - \frac{k_b + k_f\exp(-K_\Sigma t)}{K_\Sigma}\Big] \tag{8}$$

Assuming that only O is present at $t = 0$ would require the application of an infinitely positive start potential before stepping to the target potential. Here, it is assumed that the start potential is sufficiently positive for the initial coverage of R to be negligible with respect to that of O. Assuming that the rate constants have a potential dependence that follows Butler-Volmer kinetics:

$$k_f = k_s\exp\Big(-\alpha\frac{nF}{RT}\eta\Big) \tag{9}$$

$$k_b = k_s\exp\Big[(1-\alpha)\frac{nF}{RT}\eta\Big] \tag{10}$$

We also considered the Marcussian kinetics formalism but it turns out, *vide infra* that the data treatment only requires target overpotentials within the range where the Butler-Volmer and Marcusian kinetics are in very good agreement [19]. To simplify the potential dependence of the charge, it is convenient to express the rate constants k_f and k_b as functions of the dimensionaless potential ϵ according to:

$$\epsilon = \exp\Big(\frac{nF}{RT}\eta\Big) \tag{11}$$

$$k_f = k_s \epsilon^{-\alpha} \tag{12}$$

$$k_b = k_s \epsilon \epsilon^{-\alpha} \tag{13}$$

At infinitely long times, Q can be expressed as:

$$Q_{lim} = Q^0\Big(1 - \frac{k_b}{k_f + k_b}\Big) = Q^0\Big(1 - \frac{\epsilon}{1+\epsilon}\Big) \tag{14}$$

which can be rearranged to give:

$$Q_{lim} = Q^0\Big(1 - \frac{1}{1 + \exp(-nF\eta/RT)}\Big) \tag{15}$$

Going one step further it can be shown that Equation 15 corresponds to the Nernst Equation:

$$E = E^0 + \frac{RT}{nF}\ln\Big(\frac{Q^0 - Q_{lim}}{Q_{lim}}\Big) \tag{16}$$

With these definitions, Equation 8 can be rearranged and simplified:

$$Q = Q^0\Big[1 - \frac{\epsilon}{1+\epsilon} - \frac{\exp(-K_\Sigma t)}{1+\epsilon}\Big] \tag{17}$$

$$Q = Q_{lim} - \frac{Q^0}{1+\epsilon}\exp(-K_\Sigma t) \tag{18}$$

noting that

$$Q_{lim} = \frac{Q^0}{1+\epsilon} \tag{19}$$

the charge Q at any given potential and time is given by:

$$Q = Q_{lim}[1 - \exp(-K_\Sigma t)] \tag{20}$$

With $j = \mathrm{d}Q/\mathrm{d}t$ and Equation 14, the current density as a function of potential and time is:

$$|j| = Q^0 k_f \exp(-K_\Sigma t) \tag{21}$$

Equations 20 and 21 respectively provide the means to predict chronocoulograms and chronoamperograms for any target potential. Similar expressions have been reported previously [2, 6, 20]. In the following sections, we exploit these expressions to construct sampled current voltammograms and sampled charge voltacoulograms (SQVs) and derive methodologies to extract the electron transfer kinetic parameters.

3. Analysis of SQVs and SCVs

Figures 1 and 2 respectively show how the charge and current depend on overpotential and time. In Figure 1, the projections on the $Q - \eta$ plane show selected sampled charge voltacoulograms (SQVs) while in Figure 2, the projections on the $j - \eta$ plane show selected sampled current voltammograms (SCVs).

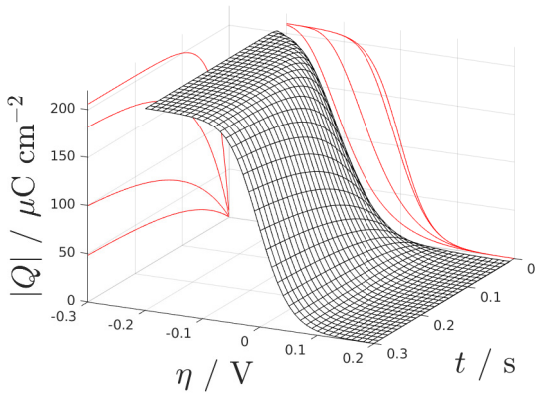

Figure 1: Dependence of the charge on η and t according to Equation 20. The parameters used were $n = 1$, $Q^0 = 210$ μC cm^{-2}, $\alpha = 0.5$ and $k_s = 5$ s^{-1}. The potentials of the selected chronocoulograms are from bottom to top: 0.03 V, 0 V, -0.05 V and -0.1 V. The sampling times for the selected sampled charge voltacoulograms are from right to left: 501 ms, 201 ms, 51 ms and 21 ms.

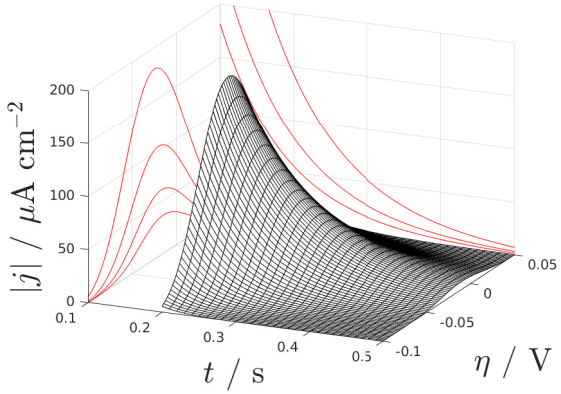

Figure 2: Current as a function of η and t from Equation 21. The parameters used were $n = 1$, $Q^0 = 210$ μC cm^{-2}, $\alpha = 0.5$ and $k_s = 5$ s^{-1}. The potentials of the selected current transients are from top to bottom: 0 V, 0.02 V and 0.03 V. The sampling times for the selected sampled current voltammograms are from top to bottom: 201 ms, 251 ms, 301 ms and 351 ms.

3.1. Analysis of the SQVs

The SQVs have a sigmoidal shape where the charge reaches a limit equal to Q^0 at large overpotentials, Equation 19. At long sampling times, the SQVs converge onto one sigmoidal wave. However, decreasing the sampling time draws the sigmoidal wave towards large overpotentials. This illustrates the sensitivity of SQVs to the electron transfer kinetics with kinetic limitations becoming very clear as the sampling time decreases. This is further illustrated in Figure 3 where SQVs calculated at 50 and 500 ms are compared. Analysing the chronocoulograms helps with the understanding of the SQVs. The chronocoulograms reach a maximum charge, Q_{lim}, which depends on the overpotential, Equations 14 and 15. This dependence corresponds to the sampled charge voltacoulogram obtained at long times. The sigmoidal wave observed

is a direct consequence of Equation 15, where the charge obtained at infinite time for a given potential depends on the relative coverage of O and R. At short times, the SQVs are drawn to more negative potentials because the sampling occurs in the rising part of the chronocoulograms; in other words, full conversion of O to R requires higher overpotentials at short sampling times.

3.2. Analysis of the SCVs

Contrary to the SCVs for diffusion controlled processes where sigmoidal waves are obtained [14, 15, 16], here, the sampled current voltammograms are peak-shaped; this can be explained in terms of the driving force. For a fixed sampling time and $E > E_{pk}$, where E_{pk} is the SCV peak potential, the reaction rate is slow because $k_f < k_b$ so only a fraction of the initial coverage has reacted by the time the current is sampled, thereby generating a small current. When $E < E_{pk}$, the rate of the reaction is fast because $k_f > k_b$ and the coverage of O decreases rapidly with more negative potentials. At the peak potential, the maximum rate results from a fast reduction and a large amount of O left to reduce. The SCV peak turns out to be very sensitive to the sampling time. As the latter decreases, the SCV currents increase exponentially according to Equation 21, the peak potential shifts to more negative values (the shift is very clear in Figure 3 where the SCVs have been normalised) and the peak becomes increasingly asymmetric, see Figure 3 and Figure S1 of the supplementary information. These observations are congruent with the scan rate dependence of the peak in conventional cyclic voltammetry.

Overall, SQVs and SCVs are found to be strongly affected by the sampling time and in the next section we exploit this dependence to extract kinetic parameters.

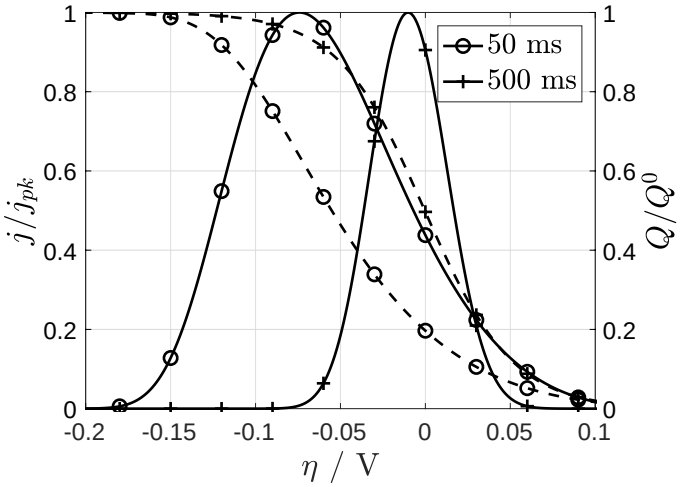

Figure 3: Normalised sampled current voltammograms (left axis, solid lines) and normalised sampled charge voltacoulograms (right axis, dashed lines) calculated with $n = 1$, $\alpha = 0.5$ and $k_s = 5$ s^{-1}.

4. Discussion

4.1. Experimental considerations

Modern electrochemical workstations are sufficiently programmable to automatically record SQVs and SCVs with a few lines of instructions in a script file. Thus, experimentally, the issue is not so much how difficult it is to acquire the data, but how long it takes. Since kinetic limitations show up at short times, fast processes will require sampling the current or charge at least every millisecond (for comparison, sampling at 1 ms affords the same time scale as a 25 V s^{-1} sweep rate in cyclic voltammetry). While a 1 s duration is generally enough to acquire current transients (the current drops to zero at long times), longer durations may be considered for chronocoulograms to ensure the charge reaches its limit Q_{lim}. A typical SCV requires 50 potential steps to record a transient every 20 mV over a 1 V wide potential window and would therefore last 500 s with a 9 s conditioning rest followed by a 1 s step. In practice, this requires stable and reproducible electrochemistry, and will depend on the reaction of interest. For example, we designed a conditioning waveform to maintain the electroactivity of the Pt electrodes when studying the impact of adsorbed oxygen species on the oxygen reduction reaction [17]. In this work, the SCVs were constructed by sampling chronoamperograms from 80 potential steps within the potential window of interest. Each current transient was acquired after conditioning the electrode with a series of voltammetric sweeps and a rest potential before stepping to the target potential. Each experiment lasted circa 40 s and the whole $i - E - t$ dataset was acquired in circa 55 min [17]. Besides providing a sensitive overview of the impact of electron transfer kinetics, the ability to include a conditioning waveform before each potential step is a key advantage of sampled current voltammetry over conventional cyclic voltammetry; this ensures that each potential step is recorded with the same electrode history. The conditioning will of course be specific to the reaction of interest and to the electrode material involved. Electrochemical conditioning is very easily implemented within the SCV procedure but one could also consider optical conditioning, e.g. by illuminating the electrode with a particular wavelength before the potential step, or chemical conditioning, e.g. by altering the pH of the electrolyte in a flow cell.

4.2. Data treatment

Equations 20 and 21 suggest two analytical approaches to extract kinetic information. Method 1 involves fitting a few experimental transients to Equations 20 or 21 for a few target potentials selected within the potential window of interest. Method 2 involves fitting a few SQVs or SCVs to Equations 20 or 21 for a few sampling times. In each case, the aim is to derive the four unknowns, Γ^0_{O}, E^0, α and k_s. Method 1 is less demanding since it only requires a small number of transients. In contrast, method 2 typically requires fifty potential steps to reconstruct the

SQV or SCV faithfully for any sampling time. However, the number of potential steps required in method 2 is actually much smaller because the target potentials can be restricted to the potential window where kinetic limitations appear, *vide infra*. Because k_f and k_b are so potential dependent, method 2 appears to be more numerically satisfying. Our group has previously shown that this approach was very convenient to extract kinetic information from SCVs recorded with microdisc electrodes [16]. With both methods, it is also possible to perform non-linear regression of the experimental transients to Equations 20 or 21 and derive the four unknowns. With modern data analysis software it is even possible to perform the non-linear regression on several datasets at the same time to improve the parameter determination. Hence, a simple approach involves recording a few transients for different target potentials and fitting the whole dataset to determine the four unknowns. In the following section, we investigate procedures to determine some of the parameters separately. To illustrate the treatment of the data, we have selected a moderately fast system ($k_s = 5$ s^{-1} and $\alpha = 0.5$) which could be easily investigated with conventional electrochemical workstations capable of acquiring transients on the millisecond timescale; results with different standard rate constants and transfer coefficients are shown in the supporting information.

4.2.1. Analysis of the chronocoulograms

It is possible to extract Q^0 (hence Γ_O^0) and E^0 by recording a series of chronocoulograms and taking their Q_{lim} values, however, Equation 15 assumes that the charge is recorded from $t = 0$ which is experimentally challenging. Moreover, the total charge also includes the contribution from the double layer capacitance. Thus, an accurate value of Q_{lim} is difficult to obtain this way. Similarly, it is possible to derive K_Σ for each target potential by fitting the chronocoulograms to Equation 20. The Tafel analysis of K_Σ, Figure 4 (right axis), presents linear branches which respectively correspond to logarithmic plots of k_f and k_b. The values of k_s and α can be obtained from the intercept and slope respectively (Equations 9 and 10). The dashed lines show the extrapolation of the linear regimes with E^0 corresponding to the potential where both lines intersect (see also Figure S2 in the supplementary information). For a process with slow kinetics this methodology may suffice; however, for a system with large k_s, obtaining K_Σ from Equation 20 can lead to errors, since it requires a wide range of overpotentials to ensure the determination of the linear branches. Furthermore, the branches only appear when $|\eta| > 0.1$ V and this requires short sampling times to ensure the reaction is kinetically limited. The determination of K_Σ in this manner also suffers from experimental limitations (need to acquire from $t = 0$) and distortion from the double layer charging process. From a data treatment point of view, the coulometric approach appears to have limited value. However, from a theoretical point of view, Equation 20 also represents the charge of a capacitor with a time constant equal to $1/K_\Sigma$. Pursuing this analogy, we can estimate that 99% of the Faradaic charge (i.e. of the final coverage) is achieved after a characteristic time $\tau = 4.6/K_\Sigma$ or $5/K_\Sigma$ for simplicity. Similarly, the double layer charging process is 99% complete after a time equal to $5RC$, where R and C are respectively the solution resistance and double layer capacitance. The sampling times must therefore be selected between these two characteristic times, i.e. within the range $5RC < t < 5/K_\Sigma$. Substituting for K_Σ and recalling Equations 11 to 13 yields $5RC < t < 5/(k_s\epsilon^{-\alpha}(1+\epsilon))$. At $\eta = 0$ this simplifies to $5RC < t < 5/(2k_s)$. Accurate kinetic information is thus available when sampling the chronoamperograms withing this timeframe. The lower limit is crucial since below $5RC$ the current is affected by capacitive distortions. The upper limit is less important; above $5/(2k_s)$ the conversion between O and R is complete and the current is equal to zero within experimental error. As K_Σ depends on potential (through k_f and k_b), so does τ. A plot of τ against overpotential (Figure 4 left axis), reveals that this characteristic time is maximised at the equilibrium potential for $\alpha = 0.5$. This shifts up to $E^0 + 25$ mV for transfer coefficients between 0.3 and 0.7 (see Figure S2 in the SI). Applying a potential in this region will therefore ensure the longest time span to determine the kinetic parameters.

In summary, it is possible to extract the relevant parameters from the experimental chronocoulograms but the quality of the data obtained is affected by the difficulty to measure accurate charges at very short times, a common problem inherent to coulometric techniques.

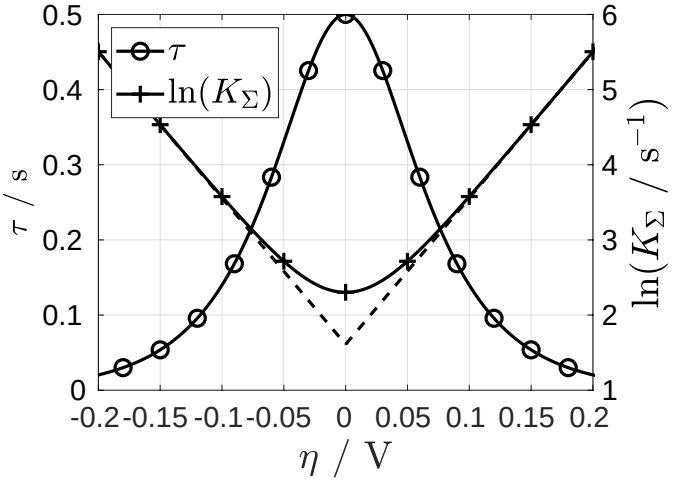

Figure 4: Plots of $\ln(K_\Sigma)$ (right axis) and τ (left axis) against η calculated with $n = 1$, $\alpha = 0.5$ and $k_s = 5$ s^{-1}. The dashed lines show the extrapolation to E^0.

4.2.2. Analysis of the SCV peaks

As mentioned above, the shape and position of the SCV peaks are very sensitive to electron transfer kinetics. As the sampling time is decreased, the peak shifts away from

the equilibrium potential and becomes increasingly asymmetric. A similar behaviour is observed with voltammetric techniques when the scan rate ν is increased and the values of k_s and α can be obtained by extrapolating the linear region observed in plots of the peak potential, E_{pk}, against $\ln(\nu)$, as originally proposed by Laviron for sweep voltammetry [1]. For the case where only the forward reaction is relevant (i.e. when $k_f >> k_b$), the dependence of the SCV peak potential and current on the sampling time are given by Equations 22 and 23 (see the supporting information for the derivation):

$$E_{pk} = E^0 - \frac{RT}{\alpha nF}\ln\Big(\frac{1}{k_s t}\Big) \tag{22}$$

$$j_{pk} = \frac{Q^0}{t}\exp(-1) \tag{23}$$

For a system that contains both forward and backward reactions, Figure S3 in the SI, it can be seen that Equation 23 only predicts the peak currents reliably at short times, i.e. when the assumption that the backward reaction does not influence the current is valid.

To obtain kinetic information, it is possible to construct an equivalent Laviron plot as E_{pk} against $\ln(1/t)$. Figure 5 shows examples obtained with different values of k_s. Using Equation 22, the value of the transfer coefficient can be readily obtained from the slope of the linear region. If E^0 is known, k_s can be derived from the linear region by deriving the characteristic sampling time t_c that corresponds to $E_{pk} = E^0$, at that point, $k_s = 1/t_c$.

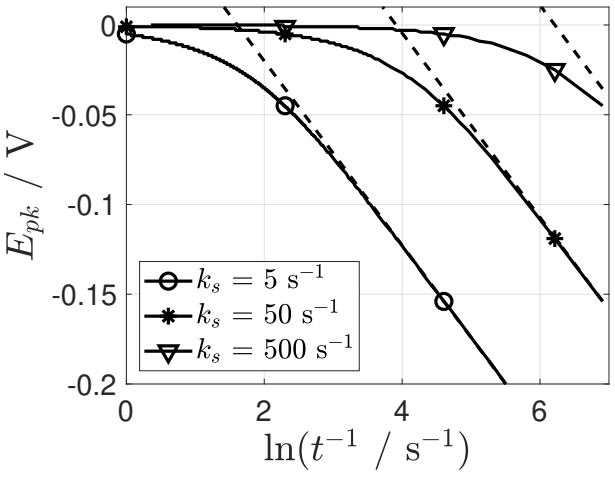

Figure 5: Equivalent Laviron plots for different rate constants. E_{pk} is the peak potential from the SCVs and t is the sampling time. SCVs obtained from Equation 21 with $Q^0 = 210$ μC cm^{-2}, $n = 1$ and $\alpha = 0.5$. The dashed line represents Equation 22 for each k_s.

This methodology is presented here as an analogy with the one proposed by Laviron for voltammetric techniques [1], and as such, it has similar constraints. Figure 5 shows that for low values of k_s, the linear region is easily observed, while larger values of k_s require shorter times that may not be accessible with general purpose potentiostats. Figure 5 also shows that an overpotential of at least 0.1 V is required to observe the linear region; this limits the highest sampling time where kinetic information can be accessed, and it requires a high number of potential steps to resolve the peaks.

The following section introduces a new methodology to obtain the four parameters irrespective of k_s without the need to resolve the peaks, i.e. without the need to apply a large number of potential steps.

4.2.3. Logarithmic SCVs

Linearising Equation 21 gives:

$$\ln(|j|) = \ln(Q^0 k_f) - K_\Sigma t \tag{24}$$

and indicates that $\ln(|j|)$ is a linear function of time. Equation 24 makes it possible to calculate $Q^0 k_f$ and K_Σ for each target potential. This is very useful because it is easily shown that the ratio $Q^0\, k_f/K_\Sigma$ follows a unique sigmoidal dependence on the target potential:

$$\frac{Q^0\, k_f}{K_\Sigma} = \frac{Q^0}{1+\exp\Big(\frac{nF}{RT}(E-E^0)\Big)} \tag{25}$$

where for increasingly large overpotentials, K_Σ tends toward k_f and $Q^0 k_f/K_\Sigma$ approaches Q^0, as shown in Figure S7 [21]. Hence, a single potential step at a large overpotential (-118 mV will ensure that the ratio is within 1% of Q^0 and there is no point applying a larger overpotential because the current magnitude drops significantly after the SCV peak as shown in Figure 2) yields Q^0 and therefore the initial charge Γ^0_O without having to rely on chronocoulograms. Once Q^0 is known, E^0 can be derived from Equation 25 using the ratio $Q^0 k_f/K_\Sigma$ from a second potential step at a lower overpotential. Alternatively, plotting the target potential against $\ln(\frac{Q^0-r}{r})$ where $r = Q^0 k_f/K_\Sigma$ produces a straight line from which E^0 can be derived. Interestingly, -118 mV is well within the range of overpotentials where the Butler-Volmer and Marcusian kinetics are in very good agreement [19].

In contrast, the dependence of $\ln(|j|)$ on potential is not obvious from Equation 24 but it is very clear when presented on a graph, Figure 6. Plotting the logarithm of the sampled current against the target potentials for different sampling times reveals visually powerful logarithmic SCVs which are highly sensitive to the sampling time. Taking the logarithm of the sampled currents increasingly flattens the SCV peaks as the sampling time decreases.

When $t = 0$, the limiting case represented with a dashed line in Figure 6, the second term in Equation 24 disappears and after substituting for k_f gives:

$$\ln(|j^0|) = \ln(Q^0 k_s) - \alpha\frac{nF}{RT}(E-E^0) \tag{26}$$

where j^0 refers to the current at $t = 0$. Equation 26 corresponds to the hypothetical case where the backward reaction is absent and it reveals that $\ln(j^0)$ is a linear function

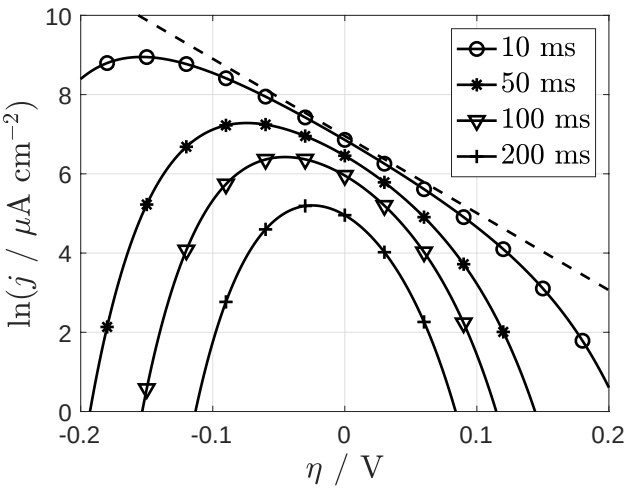

Figure 6: Logarithmic sampled current voltammograms calculated with $n = 1$, $\alpha = 0.5$, $k_s = 5\ \mathrm{s}^{-1}$ and $Q^0 = 210\ \mu\mathrm{C\ cm}^{-2}$. The dashed line represents the irreversible case, Equation 26. Additional cases are presented in Figures S4 and S5 in supplementary information.

of potential, as shown by the dashed line in Figure 6. For additional cases see Figure S6 in supplementary information. The slope of a plot of $\ln(j^0)$ against the target potential can then be used to determine α [22], which can also be used to determine E^0 once α is known. Subsequently, the intercept of Equation 26 can be used to determine k_s since the other three parameters are now known. The same two transients employed to derive Q^0 and E^0 can be used to derive α and k_s. In effect, extrapolation to $t = 0$ bypasses the timeframe where the current is affected by the double layer charging process. We can estimate the largest measurable k_s value by assuming that the time to complete the Faradaic process, $5/(2k_s)$, is equal to 10 times the time to reorganise the double layer ($5RC$). For a typical set of conditions, an electrolyte conductivity of $6.3\text{x}10^{-2}\ \Omega^{-1}\ \mathrm{cm}^{-1}$ (typical for a 0.5 M NaCl solution), an electrode capacitance of 20 μF cm^{-2} (typical for Pt), and a surface roughness of 3 (typical when polishing with 0.3 μm Al_2O_3), the largest measurable k_s would range from circa $4\text{x}10^5\ \mathrm{s}^{-1}$ with a 1 μm diameter Pt disc to circa $3\text{x}10^2\ \mathrm{s}^{-1}$ with a 1 mm diameter Pt disc [23]. The upper value is consistent with those previously recorded for adsorbed osmium complexes with microdisc electrodes [10, 24]. Higher rate constants could be determined with a less stringent criterion and smaller electrodes. For example, a rate constant circa $8\text{x}10^6\ \mathrm{s}^{-1}$ could be obtained with a 100 nm radius disc when using $5/(2k_s) = 2\text{x}(5RC)$ as the criterion (the conductivity, superficial capacitance and roughness factors are as above). We are not aware of other methods capable of determining such rate constants.

In summary, analysis of the time dependence of the current for at least two target potentials yields Q^0 and E^0 while subsequent analysis of the potential dependence of the current extrapolated to an infinitely short sampling time yields the kinetic parameters α and k_s.

4.2.4. Data treatment recipe

This section summarises two protocols we propose to derive the four unknowns from the analysis presented in Section 4.2.3. The first protocol relies on non-linear regression of the dataset to Equation 21. The second protocol exploits Equations 24 to 26 instead. In both cases, we assume that the potential window will already be known from a cyclic voltammogram either previously recorded or from the literature, and that the anodic and cathodic peak potentials, respectively E^a_{pk} and E^c_{pk} will have been noted.

Protocol 1:

1. Record current transients for several target potentials across the potential window of interest. Transients holding 1000 data points over 1 s should suffice for most cases but higher acquisition rates may be needed for very fast processes. Two target potentials are enough to determine the four unknowns. One should be selected near the peak potential for the forward reaction and the other should correspond to a large overpotential (ideally $|\eta| > 118$ mV), for example $(E^a_{pk} + E^c_{pk})/2 - 120\,\mathrm{mV}$ to facilitate the determination of Q^0. Additional target potentials selected within the potential window will help firm up the unknown values.
2. Determine, e.g. using Origin, the four unknowns by non-linear regression of the global dataset (the set of current transients recorded for the different target potentials) to Equation 21. Fitting all the transients at the same time ensures that the time and potential dependences are taken into account. Fitting the transients one at a time would weaken the dependence of the current on the target potentials.

Protocol 2:

1. Record at least two current transients for two target potentials as in step 1 above.
2. Take the logarithm of the chronoamperograms and, using Equation 24, derive K_Σ and $Q^0 k_f$ for each target potential.
3. Determine Q^0 from the ratio $Q^0\,k_f/K_\Sigma$ corresponding to the transient recorded for a large overpotential, then derive Γ^0_{O} from Q^0.
4. Derive E^0 using Q^0, the ratio from the second transient and Equation 25. If transients have been recorded for more target potentials, Q^0 and E^0 can instead be determined from a plot of the ration $Q^0 k_f/K_\Sigma$ against the target potentials where E^0 is the potential where the ratio equals $Q^0/2$.
5. Extrapolate each logarithmic transient to $t = 0$ and derive $\ln(j^0)$ for each target potentials using Equation 24.
6. Derive α from the slope of $\ln(j^0)$ against target potentials using Equation 26.
7. Derive k_s from the intercept of $\ln(j^0)$ against target potentials using Equation 26 and the values of the other three parameters.

It is also possible to perform protocol 2 first, then step 2 of protocol 1. This way, the values of Q^0, E^0, α and k_s can be used as initial guesses to constrain the non-linear regression.

5. Conclusions

Here we discussed the use of sampled current voltammetry to study the kinetics of electron transfer involving adsorbed species in the absence of diffusion. The voltammograms obtained are peak-shaped and although they can be analysed with an equivalent Laviron plot to calculate kinetic parameters, this requires a large number of target potentials. Instead, we proposed two protocols, a simple one involving non-linear regression of the dataset to Equation 21 and an alternative involving the analysis of chronoamperograms using Equations 24 to 26. In the latter case, two current transients are sufficient to determine the four unknown parameters. Here, the only constraint is that one of the chronoamperograms must be recorded with a large overpotential. The time dependence of the current transients yields Q^0, Γ_O^0 and E^0, while the potential dependence of the current extrapolated to $t = 0$ yields α and k_s. The key aspect of the second protocol, taking the logarithm of the transients, makes it possible to extrapolate the currents to an infinitely short sampling time where the backward reaction is absent. Importantly, this extrapolation bypasses the timescale where the experimental current is distorted by the double layer charging process.

The analysis of the chronoamperograms has clear advantages over traditional voltammetry. 1) The double layer charging process only affects the current transients at short times whereas it affects the whole potential window in voltammetry. 2) The current transients can be extrapolated to very short sampling times where the backward reaction has no influence. This can be seen graphically in logarithmic SCVs which are more sensitive to k_s than normal SCVs. 3) The extrapolation to very short sampling times alleviates the need to subtract the double layer distortion. 4) While a typical chronoamperogram covers all required timescales to distinguish the kinetic regimes, the voltammetric approach requires a wide range of scan rates to do the same. 5) The voltammetric method only yields the values of k_s and α, while the chronoamperometric method also yields Γ_O^0 and E^0. 6) In most electrochemical workstations, shorter experiment timescales can be achieved by chronoamperometry than by voltammetry, thus the chronoamperometric approach makes it possible to study faster electrode reactions. Overall, we believe that the chronoamperometric method is easy to implement, works well with conventional electrochemical workstations, is applicable to any electrode size and can probe faster electrode kinetics than the traditional voltammetry with the Laviron approach.

6. Acknowledgements

O.R. thanks CONACYT-I2T2 for the scholarship provided (No. 411294) to pursue a PhD in Chemistry at the University of Southampton.

References

[1] E. Laviron, General expression of the linear potential sweep voltammogram in the case of diffusionless electrochemical systems, Journal of Electroanalytical Chemistry and Interfacial Electrochemistry 101 (1) (1979) 19–28.

[2] J. J. ODea, J. G. Osteryoung, Characterization of quasi–reversible surface processes by square–wave voltammetry, Analytical Chemistry 65 (21) (1993) 3090–3097.

[3] H. A. Heering, M. S. Mondal, F. A. Armstrong, Using the pulsed nature of staircase cyclic voltammetry to determine interfacial electron-transfer rates of adsorbed species, Analytical Chemistry 71 (1) (1999) 174–182.

[4] M. A. Mann, L. A. Bottomley, Cyclic square wave voltammetry of surface–confined quasireversible electron transfer reactions, Langmuir 31 (34) (2015) 9511–9520.

[5] C. Montella, Further investigation of the equivalence of staircase and linear scan voltammograms. III-averaged-current staircase voltammetry applied to electrochemical reactions involving adsorbed species, Journal of Electroanalytical Chemistry 808 (2018) 348–361.

[6] J. González, N. Abenza, Á. Molina, Analytical solutions of the multipotential pulse quasi-reversible Q–E–t and I–E–t responses of strongly adsorbed redox molecules, Journal of Electroanalytical Chemistry 596 (1) (2006) 74–86.

[7] N. Abenza, J. Gonzalez, A. Molina, General behavior of the I–E and ΔI–E curves obtained when a multistep potential is applied to an electroactive monolayer, Electroanalysis 19 (9) (2007) 936–944.

[8] C. G. Zoski, Charging current discrimination in analytical voltammetry, Journal of Chemical Education 63 (10) (1986) 910.

[9] D. Acevedo, H. D. Abruna, Electron-transfer study and solvent effects on the formal potential of a redox-active self-assembling monolayer, The Journal of Physical Chemistry 95 (23) (1991) 9590–9594.

[10] R. J. Forster, L. R. Faulkner, Electrochemistry of spontaneously adsorbed monolayers. Equilibrium properties and fundamental electron transfer characteristics, Journal of the American Chemical Society 116 (12) (1994) 5444–5452.

[11] R. J. Forster, Microelectrodes: new dimensions in electrochemistry, Chemical Society Reviews 23 (4) (1994) 289.

[12] R. J. Forster, Electron transfer dynamics and surface coverages of binary anthraquinone monolayers on mercury microelectrodes, Langmuir 11 (6) (1995) 2247–2255.

[13] C. Zuliani, D. A. Walsh, T. E. Keyes, R. J. Forster, Formation and growth of oxide layers at platinum and gold nano- and microelectrodes, Analytical Chemistry 82 (17) (2010) 7135–7140.

[14] M. V. Mirkin, A. J. Bard, Simple analysis of quasi–reversible steady–state voltammograms, Analytical Chemistry 64 (19) (1992) 2293–2302.

[15] Y.-J. Deng, G. K. H. Wiberg, A. Zana, M. Arenz, On the oxygen reduction reaction in phosphoric acid electrolyte: Evidence of significantly increased inhibition at steady state conditions, Electrochimica Acta 204 (2016) 78–83.

[16] S. C. Perry, L. M. A. Shandoudi, G. Denuault, Sampled-current voltammetry at microdisk electrodes: Kinetic information from pseudo steady state voltammograms, Analytical Chemistry 86 (19) (2014) 9917–9923.

[17] S. C. Perry, G. Denuault, Transient study of the oxygen reduction reaction on reduced Pt and Pt alloys microelectrodes: evidence for the reduction of pre–adsorbed oxygen species linked to dissolved oxygen, Physical Chemistry Chemical Physics 17 (44) (2015) 30005–30012.

[18] C. O. Soares, O. Rodríguez, G. Buvat, M. Duca, S. Garbarino, D. Guay, G. Denuault, A. C. Tavares, Sampled current voltammetry for kinetic studies on materials unsuitable for rotating discs or microelectrodes: Application to the oxygen reduction reaction in acidic medium, Electrochimica Acta 362 (2020) 136946.

[19] C. E. D. Chidsey, Free energy and temperature dependence of electron transfer at the metal-electrolyte interface, Science 251 (4996) (1991) 919–922.

[20] S. E. Creager, K. Weber, On the interplay between interfacial potential distribution and electron-transfer kinetics in organized monolayers on electrodes, Langmuir 9 (3) (1993) 844–850.

[21] Comparing Equation 25 with Equation 15 reveals that the ratio $Q^0 k_f/K$ is in fact the same as Q_{lim}.

[22] In Section S3 of the supplementary information, we derive a unique relationship between E^0 and α, $E^0 = E - \frac{RT}{nF}\ln\left(\frac{\alpha}{1-\alpha}\right)$.

[23] The uncompensated solution resistance for the microdisc and large electrode were calculated using $R_u{=}1/(\kappa a)$ and $R_u = x/(\kappa\pi a^2)$ respectively with κ the conductivity, a the disc radius and x (here taken as 2 mm) the distance between the electrode and the tip of the Luggin capillary.

[24] R. J. Forster, L. R. Faulkner, Electrochemistry of spontaneously adsorbed monolayers. Effects of solvent, potential, and temperature on electron transfer dynamics, Journal of the American Chemical Society 116 (12) (1994) 5453–5461.